A log-log plot of $f_{RCW}(t)$ vs. t is shown as the solid line in fig. 13.1. In this and succeeding plots, the logarithms are base 2. The curve was computed numerically using an ensemble of $M = 10,000$ particles. The curve is of the form $f_{RCW}(t) = f_{RCW}(1) \cdot t^{-\alpha(t)}$ with $\alpha(t) \to \frac{1}{2}$ as $t \to \infty$. For finite time, $\alpha(t) < \frac{1}{2}$, so that $f_{RCW}(t)$ shows a slowly downward curving "backbone" whose slope approaches $-\frac{1}{2}$ as $t \to \infty$. A phenomenological model that gives a reasonable summary of $f_{RCW}(t)$ uses $\alpha(t) = \frac{1}{2}(1 - at^{-b})$ with $a = 0.8$, $b = 0.15$, and $f_{RCW}(1) = 0.22$.

The $\alpha(t) \to \frac{1}{2}$ convergence can be readily understood. An initial RCW ensemble equivalent to dislocation pairs all starting at the same separation $d(0) = 1$ decays like $f_{RCW}(t) \propto t^{-\alpha}$ with $\alpha \approx \frac{1}{2}$ for all t. The form of $f_{RCW}(t)$ observed for the exponentially distributed vicinity ensemble is roughly a superposition of the individual decays shifted by the time it takes for the particles to first begin annihilating; the latter is a function of the initial dislocation separation. And so, the decay profile slope gradually decreases until $\alpha = \frac{1}{2}$.

As described, the initial fraction of "active" RCW pairs is $f_{RCW}(0) = \frac{1}{2}$, whereas the initial fraction of ECA 18 dislocations is $f_P(0) = \frac{1}{4}$. This is due to the fact that an ECA 18 state is perturbed off the attractor with probability $\frac{1}{2}$, so that only half of the states in the vicinity ensemble ever participate in the simulation. This is only a difference in normalization, and is corrected in all of the figures.

In comparing the stochastic model to ECA 18, we will be considering the evolution of dislocations on finite lattices with periodic boundary conditions. For even-size lattices, there are two dislocations, which may annihilate either by approaching each other or by diverging from each other until they wrap around the periodic boundary; for odd lattice size, there are three dislocations, any two of which may annihilate. We treat these two cases as separate modifications of the RCW model. A general model, applicable to any number of dislocations, is a straightforward extension. However, since the vicinities we are studying have only two or three dislocations, the general model is unnecessary and is left for development elsewhere.

For two dislocations, the simpler case, we can include the finite-N effects by adding another "cliff" at lattice-site $N/2$ (the factor of $\frac{1}{2}$ comes from the RCW lattice constant, which is $\frac{1}{2}$). The resulting model is a one-dimensional *random mesa walker* (1D RMW), which has an explicit dependence on the lattice size. The model's one-dimensional nature is emphasized to differentiate it from the two-dimensional random mesa walker developed below. For an exponential distribution of initial dislocation distances $d(0)$ as above, we expect the fraction of surviving dislocations, $f_{RMW}(t)$, to show an early epoch during which it follows $f_{RCW}(t)$, followed by a gradual transition to a second epoch during which $f_{RMW}(t)$ decays at a faster rate. The transition to the second epoch occurs when the random walkers have had sufficient time to reach the second cliff at site $N/2$. Since the root-mean-square excursion $\sigma = \sqrt{\langle d^2 \rangle}$ of a single random walker evolves as $\sigma \propto \sqrt{t}$, the transition time T_d should vary with lattice size as $T_d \propto N^2$.

1D RMW decay profiles $f_{RMW}(t)$ vs. t for lattices $N \in \{32, 512\}$ are plotted on a log-log scale as dotted lines in fig. 13.1. For both lattice sizes, the curves were computed numerically using an ensemble of $M = 12,800$ particles. As the figure shows, $f_{RMW}(t)$ follows $f_{RCW}(t)$ up to a deviation time $t \approx T_d$. Numerical experiments on lattices $N \in \{2^k : 3 \leq k \leq 9\}$ indicated that T_d varies with lattices size as

$$T_d(N) = kN^2 \tag{13.9}$$

with $k \approx 0.07$. At T_d there is a gradual transition to a faster decay rate. The decay in the second epoch is roughly exponential, with a rate that decreases as N grows larger. In fig. 13.1 the transition to the second epoch shows up as a smooth downturn of $f_{RMW}(t)$ away from $f_{RCW}(t)$.

The case with three dislocations, corresponding to ECA 18 on an odd-size lattice, requires a more complex modification, since there are three possible ways for the dislocations to annihilate. We can express the evolution in terms of any two of the three interdislocation distances, i.e., $d_1(t)$ and $d_2(t)$. These move according to the stochastic evolution equation

$$\begin{aligned} d_1(t) &= d_1(t-1) + \delta_1 \\ d_2(t) &= d_2(t-1) + \delta_2 \end{aligned} \tag{13.10}$$

where δ_1 and δ_2 are random variables with values in $\{-1, 0, +1\}$ and with a joint distribution $p(\delta_1, \delta_2)$ given by

$$\begin{aligned} &p(0,0) = 1/4 \\ &p(-1,-1) = p(+1,+1) = 0 \\ &\text{All others} : p(\delta_1, \delta_2) = 1/8 \end{aligned} \tag{13.11}$$

The evolution is subject to the constraints

$$\begin{aligned} &d_i(t) > 0, \quad i = 1, 2 \\ &d_1(t) + d_2(t) < (N-1)/2 \end{aligned} \tag{13.12}$$

Violation of any of these constraints signifies that a pair of random walkers has annihilated, and so evolution stops at that point. In effect, this is a random walk in two dimensions on a triangular mesa, i.e., a 2D RMW on the simplex defined by eq. 13.12. The initial distribution corresponding to Hamming-vicinity decay in ECA 18 has $d_1(0)$ distributed exponentially as for the 1D RMW, and $d_2(0)$ uniform over the interval $1 \leq d_2(0) \leq (N-1)/2$. Note that a portion of this distribution lies off the simplex, so that some random walkers are already beyond the edge at time zero; this is the same as for ECA 18.

The dashed lines in fig. 13.1 show the 2D RMW decay profiles $f_{RMW}(t)$ vs. t for lattices $N \in \{33, 513\}$. As for the 1D RMW profiles, the curves were computed numerically using an ensemble of $M = 12,800$ particles. The curves do not follow the RCW backbone, but rather start some distance below the backbone and curve smoothly downward. The time-1 fraction $f_{RMW}(1)$ varies with lattice size roughly as

$$f_{RMW}(1) \approx c_1 - c_2/N \tag{13.13}$$

with $c_1 = 0.22$ and $c_2 = 1.0$. For each N, the 2D RMW decay profile lies below the corresponding 1D RMW curve, indicating a faster decay rate. As for the 1D RMW case, the decay becomes roughly exponential after an initial epoch. The transition to exponential decay sets in earlier and is much more gradual, making a divergence time more difficult to specify. However, the long-time behavior indicates that the transition has the same lattice-size dependence as does the 1D RMW. This can be observed in fig. 13.1 by noting that the exponential tails of the 1D and 2D decay profiles for lattices $N \in \{512, 513\}$ are offset by the same amount as for $N \in \{32, 33\}$. Data from lattices $N \in \left\{2^k + 1 : \; 3 \leq k \leq 10\right\}$ indicate that, in the exponential decay epoch, a 2D RMW with lattice size N follows approximately the same curve as a 1D RMW on a lattice of size $N/2$.

If ECA 18 Hamming vicinity decay mimics ideal diffusive annihilation, then its behavior should agree with the 1D RMW stochastic process on even-size lattices, and with the 2D RMW process on odd-size lattices. The temporal decay $f_P(t)$ should follow the same curve as the appropriate $f_{RMW}(t)$. Conversely, deviations from random mesa walker profiles must be ascribed to other decay mechanisms and state space structures than diffusive annihilation on a finite lattice with periodic boundary conditions. As we show in the next section, Hamming vicinity decay of ECA 18 typically mimics the stochastic process quite well throughout most of its evolution.

13.3 Hamming Vicinity Decay

Returning now to our investigation of the stability of ECA 18's attractors, we study the temporal relaxation of the Hamming vicinity back onto the attractor in relation to the stochastic decay models. As discussed above, the Hamming vicinity is the physically realistic vicinity to use, since it traces the response of the system to spatially local perturbations.

Hamming vicinity decay for ECA 18 was investigated for a number of lattice sizes $N < 1000$, largely chosen arbitrarily. For each lattice, an initial vicinity ensemble was created as described in section 13.1. At each time step each pattern in the ensemble was iterated once. The number of dislocations in each state s was counted using the machine metric $\|\mathrm{s}\|_{\mathrm{M}(\Lambda^o)}$. When the number fell below two, that pattern was removed from the ensemble, since it was on the attractor. States with two or more dislocations were allowed to continue evolving until their dislocations annihilated or they were proven to be on a periodic orbit. The latter condition was detected using a method described in [67]. At each time, the fraction $f_\Lambda(t)$ of states on the attractor was measured, and the nonattracted fraction $f_P(t)$ was calculated according to $f_P(t) = 1 - f_\Lambda(t)$. Vicinity ensemble sizes of $M_1 = 2 \times 10^4$, $M_2 = 1 \times 10^5$, and $M_3 = 1 \times 10^6$ were used. For $N > 500$ the ensembles were all of the size M_1; otherwise the size was chosen arbitrarily between M_2 and M_3, and appeared to have little effect on the results, other than reducing statistical fluctuations in the estimated fractions at large times.

We investigated 12 lattice sizes selected from the following groups.

1. Worst case.[62] As we will see, the lattices with the largest asymptotic fraction f_P are those with $N_k = 3 \cdot 2^k - 2, k = 0, 1, 2, \ldots$. Since the difference in size between lattices grows exponentially, the worst-case lattices comprise a sparse set. We chose the subset $N_{wc} = \{22, 46, 94, 190, 382, 766\}$.
2. Winding number $\omega = 0$. The winding number ω is the "rotation rate" of spatial patterns on temporally periodic orbits of a finite lattice.[65] Since the nonattracted orbits in the vicinity are all temporally periodic, we initially hypothesized that the winding number might affect the statistics of vicinity convergence. Of the lattices with $\omega = 0$ we chose the subset $N \in \{20, 24, 36\}$.
3. Winding number $\omega = 1$: $N \in \{14, 31, 42\}$.

In addition to the above groups, we collected the same statistics on a larger set of 22 arbitrarily selected lattice sizes: even lattices

$$N_e = \{32, 34, 66, 178, 530, 536, 598, 790, 840, 880\} \tag{13.14}$$

and odd lattices

$$N_o = \{27, 45, 77, 95, 99, 213, 629, 693, 781, 799, 879, 919\}. \tag{13.15}$$

Not surprisingly, the decay profiles $f_P(t)$ for even-size lattices showed a characteristic shape different from that of N odd. We label these two classes (I) even-N, and (II) odd-N. In addition, the even-N lattices fell into two distinct subclasses: (IA) decelerating-decay and (IB) catastrophic-decay. Classes IA, IB, and II are shown respectively in figs. 13.2, 13.3, and 13.4.

All of the even-N lattices follow a common backbone for the early part of their evolution. This backbone closely follows the stochastic RCW decay profile $f_{RCW}(t)$; the latter is plotted as a dashed line in all three figures. For example, in fig. 13.2, the backbone appears as a solid curve lying just below the dashed RCW curve. The time-1 fraction $f_P(1)$ is the same for all lattices in classes IA and IB, but differs from $f_{RCW}(1)$ by 15%. In addition, the random cliff walker decays slightly more quickly than the ECA 18 backbone, so that the difference between the two grows less with time. Lattices in class IA remain on the backbone until they approach their asymptotic values. In class IB, each lattice shows a marked downturn away from the backbone before convergence. For nearly all of these catastrophic-decay lattices (with exceptions noted below), this downturn coincides with the RMW's transition to its second (exponential) decay epoch. The convergence of the curves to nonzero values of $f_P(t)$, in fig. 13.2 and subsequent figures, is due to periodic orbits in the vicinity

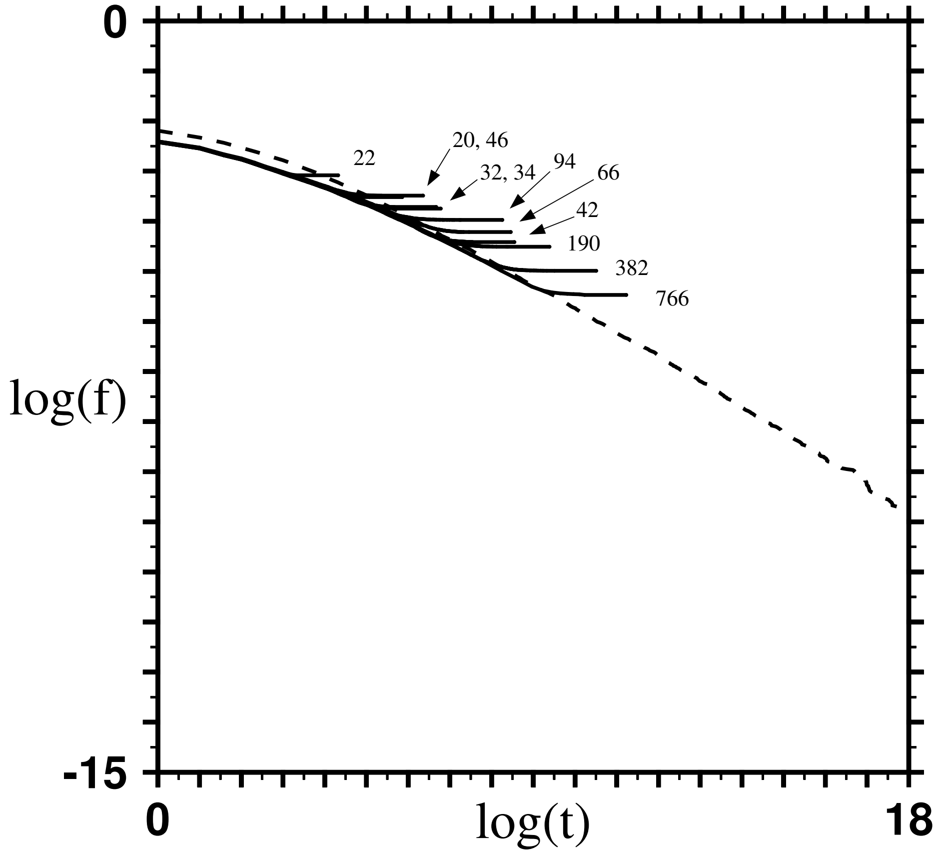

Fig. 13.2 Decelerating decay (class IA): $f_P(t)$ for lattice sizes $N \in \{20, 22, 32, 34, 42, 46, 66, 94, 190, 382, 766\}$. All curves are labeled by lattice size and plotted to $t = 2T_c$. For reference the dashed line gives the rescaled random cliff walker decay $f_{RCW}(t)$.

that do not fall back onto the attractor. The RCW and RMW models do not capture such structure, and so $f_{RCW}(t)$ and $f_{RMW}(t)$ continue to decay indefinitely.

The lattices in class IA, the decelerating-decay class, were

$$N \in \{20,\ 22,\ 32,\ 34,\ 42,\ 46,\ 66,\ 94,\ 190,\ 382,\ 766\}. \tag{13.16}$$

Fig. 13.2 shows a log-log plot of the nonattracted fraction $f_P(t)$ vs. t for these lattices. Lattices in this class follow the common backbone of class I lattices for nearly all of their evolution. Near the convergence time T_c there is a gentle leveling as the decay curve makes its final approach to a nonzero asymptotic value. In the figure, the curves have been plotted up to $t = 2T_c$ to show the values of f_P. Within the overall class, T_c appears to be roughly proportional to lattice size, and so f_P approaches 0 in the limit of large N. The worst-case lattices N_{wc}, whose asymptotic nonattracted fractions are maximal, fall into the decelerating-decay class.

This class can be characterized as having early convergence, since T_c of each lattice is less than the RMW transition time T_d. The asymptotic fraction is reached before the transition to the second stochastic epoch can occur. For lattices in class

IA, the evolution begins to diverge from the stochastic model only during the final approach to the asymptotic limit.

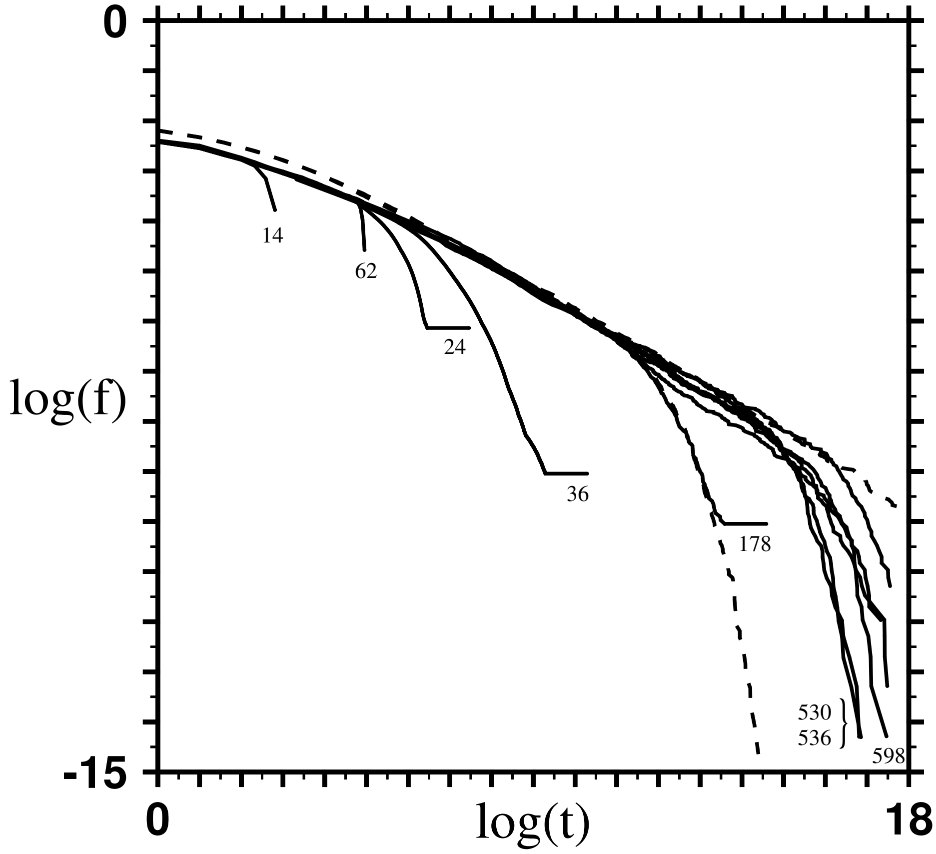

Fig. 13.3 Catastrophic decay (class IB): $f_P(t)$ for lattice sizes $N \in \{14,\ 24,\ 36,\ 62,\ 178,\ 530,\ 536,\ 598,\ 790,\ 840,\ 880\}$. Curves for all but the largest three rightmost curves are labeled by lattice size. Lattices $N \in \{24, 36, 178\}$ have nonzero f_P and are plotted to $t = 2T_c$. The three rightmost curves, from top to bottom $N \in \{840, 790, 880\}$, are plotted to the cutoff time $t = 240,000$. The remaining curves have $f_P = 0$ and are plotted to $t = T_c - 1$. For reference the upper dashed line gives the random cliff walker decay $f_{RCW}(t)$. In addition, the random mesa walker decay profile for $N = 178$ is shown as the dashed line leading off the bottom of the figure.

Fig. 13.3 shows $f_P(t)$ for class IB, catastrophic decay. The lattices shown are

$$N \in \{14,\ 24,\ 36,\ 62,\ 178,\ 530,\ 536,\ 598,\ 790,\ 840,\ 880\}. \tag{13.17}$$

As for class IA, $f_P(t)$ for these lattices initially follows the even-N backbone. At some point there is a transition to a markedly higher decay rate as seen in the profiles' downturn, which continues up to the convergence time. The time at which the transition occurs is within a few per cent of the RMW transition time T_d on larger lattices, and within a factor of two on the smaller ones. The asymptotic nonattracted fraction f_P can be zero or a finite value. As for class IA, the lattices with nonzero

f_P are indicated by horizontal tails extending to $t = 2T_c$. The three rightmost curves, $N \in \{790, 840, 880\}$, were still decaying when the evolution was stopped at $t = 240,000$. The remaining curves have $f_P = 0$, and are plotted to $t = T_c - 1$.

Two exceptional lattices, $N \in \{14, 62\}$, are included in the catastrophic-decay class, even though they converge before the RMW transition time T_d for those lattices. These are the leftmost two downward-pointing curves in fig. 13.3. These lattices are members of the sparse set for which all states in the vicinity evolve to the null state 0^* (see also section 12.2). These lattices have size $N = 2^k - 2,\ k = 2, 3, \ldots$. Since the null state is in the attractor, $f_P = 0$ for these lattices. The sharp downturn in these curves is due to the sudden decay to 0^* at time $T_c = (N + 2)/2$.

Superimposed on the decay curve for $N = 178$ is the random mesa walker decay profile $f_{RMW}(t)$ for that lattice size. It is shown as the dashed line leading off the bottom of the plot. The agreement between the two curves is remarkable; they overlap nearly all the way to T_c. This is typical of the larger class IB lattices. Smaller lattices tend to diverge from the corresponding RMW curves before T_c. As for class IA, typical lattices in class IB closely agree with the RMW stochastic model for nearly all of their evolution.

The odd-size, class II, lattices

$$N \in \{27,\ 31,\ 45,\ 77,\ 95,\ 99,\ 213,\ 629,\ 693,\ 781,\ 799,\ 879,\ 919\} \tag{13.18}$$

plotted in fig. 13.4, show the same downward curve as the decelerating decay class, except that they appear to decay more quickly than even lattices of similar size. Some of the lattices have overlapping $f_P(t)$; for example, $N \in \{95, 99\}$ lie atop one another until the latter converges to $f_P = 0.0035$, and the lattices $N \in \{629, 693, 781, 799\}$ overlap throughout their evolution. Those lattices with nonzero f_P are plotted with horizontal tails to $t = 2T_c$, as for classes IA and IB; all others have $f_P = 0$.

The time-1 fraction $f_P(1)$ varies with lattice size with roughly the same form as for the 2D RMW, i.e., $f_P(1) \approx c_1 - c_2/N$, with $c_1 \approx 0.19,\ c_2 \approx 1.2$. However, $f_P(1) < f_{RMW}(1)$ for all lattices; in this, class II is similar to class I. In general, comparison with the 2D RMW decay curves shows that most lattices follow in parallel with the stochastic-model profiles, differing from them by a roughly constant factor. A typical lattice showing this effect is $N = 213$, for which $f_{RMW}(t)$ is plotted in fig. 13.4 as a dashed line leading off the bottom of the figure. The ECA 18 decay curve for $N = 213$ runs parallel to it until the final approach to the asymptotic fraction. For some lattices, e.g. $N \in \{95,\ 99\}$, the agreement between $f_P(t)$ and $f_{RMW}(t)$ is nearly perfect.

In summary, then, the Hamming vicinity decay profiles agree well with the appropriate random mesa walker model, up until the final approach to the asymptotic value f_P. The agreement is increasingly good for larger N. Even-size lattices differ primarily in whether this limit is reached before or after the transition to the second (exponential) epoch of RMW decay. For decelerating-decay (class IA), the

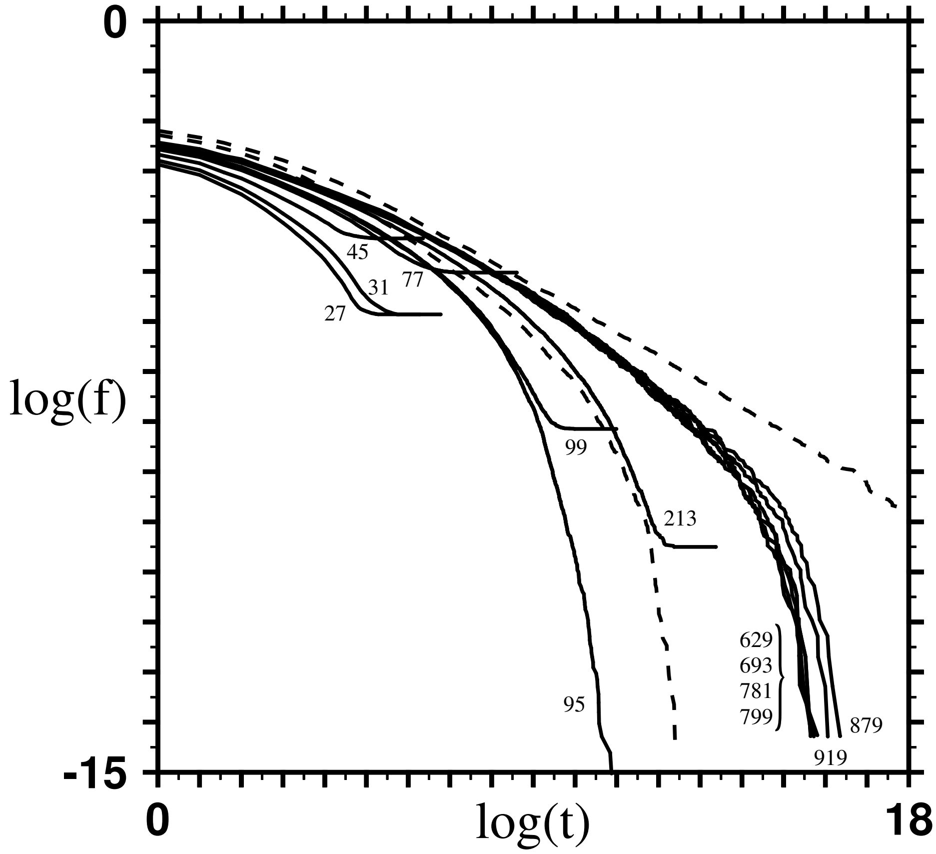

Fig. 13.4 Odd-N (class II): $f_P(t)$ for lattice sizes $N \in \{27, 31, 45, 77, 95, 99, 213, 629, 693, 781, 799, 879, 919\}$. All curves are labeled by lattice size. Lattices with nonzero f_P are plotted to $t = 2T_c$; all others are plotted to $t = T_c - 1$. The dashed line lying above all of the decay profiles is the random cliff walker decay $f_{RCW}(t)$. The 2D RMW curve for $N = 213$ is visible as a dashed line curving downward toward the bottom of the plot.

convergence time T_c is less than the RMW transition time T_d, and the asymptotic fraction f_P is nonzero. For catastrophic-decay (class IB) $T_c > T_d$, and f_P is very small or zero. On odd-size lattices, the quantitative agreement with the stochastic model is less good, although the 2D RMW does capture the shapes of the decay curves.

The fact that the decay profiles fall into only a few classes gives some hope to simply describing the geometry of the discrete state space using the qualitative dynamics analysis of chapter 12 in conjunction with statistical methods. We sketch the beginnings of such a description here; a detailed analysis will require connecting the discrete state space view with the qualitative dynamics analysis we have used. Recall the discussion at the end of section 13.1 above, which indicated that the convergence time T_c is equal to the length of the longest transient starting in the vicinity, and the instantaneous decay rate $\Delta f_P(t)$ is the same as the probability density of transient lengths. Applying this to the observed decay profiles of the three classes, we see from the convergence times T_c that lattices in class IA have relatively short transients, while for classes IB and II, there exist transients that are much longer: for example, compared to the class IA lattice $N = 766$, class IB lattice $N = 790$ and class II lattice $N = 781$ have transients that are about 500 and 100 times longer, respectively. For all lattices, linear plots of $f_P(t)$ vs. t show that $\Delta f_P(t)$ decreases quickly to zero with t. This is especially true of lattices in classes IB and II, for which $\Delta f_P(t)$ decreases exponentially during the second epoch of their evolution. Thus the distribution of transient lengths is sharply peaked at small values; there are many more short transients than long ones. Furthermore, the close agreement between the Hamming vicinity decay and the random mesa walker profiles shows that for each of classes I and II, the distribution of transient lengths up to the cutoff at T_c is well-approximated by a single family of functions parametrized by N.

Finally, the decay profiles did not indicate any great dependence on lattice winding number ω, except that $\omega = 0$ lattices decay more rapidly than comparable $\omega = 1$ lattices.

13.4 Noisy Lattices

As a second method of examining the typical behavior of ECA 18, we added a small amount of random noise to the iteration rule. The extent to which this affects the vicinity convergence profile $f_P(t)$ gives an indication of the stability of the orbits under this perturbation: in particular, of the periodic orbits off the attractor.

The random noise took a particular form, chosen specifically to be the "minimal" perturbation to a state in the vicinity. At each time step, domain wild-card cells are flipped with i.i.d. probability p_{flip}. The latter is set so that approximately one cell in the lattice is flipped per iteration, i.e., $p_{flip} \approx 2/N$ since there are approximately $N/2$ wild-card cells in a vicinity state. This perturbation does not change the number or the positions of the dislocations. Tracing the convergence profile for noisy evolution addresses the question of whether such a weak perturbation is sufficient to destroy the nonattracted periodic orbits, or whether they are stable, i.e., whether they are themselves attractors.

The overall expectation is that the noise should not affect the decay behavior in the early diffusive epoch. During the later epoch, when the statistics of the noise-free evolution are dominated by the periodic orbits, the stability of those orbits will determine the effect of the noise. If the periodic orbits are unstable, then the asymptotic fraction f_P should decay to zero. Furthermore, the differences in the shape of $f_P(t)$ for different lattices sizes should be less pronounced.

We gathered statistics for ten lattices

$$N \in \{31, 36, 42, 45, 66, 94, 190, 213, 536, 693\} \tag{13.19}$$

using ensembles of size $M = 1 \times 10^4$. This group includes examples of all three decay classes defined above. $f_P(t)$ is plotted for these lattices in fig. 13.5. Lattices

$N \in \{536, 693\}$ are plotted to $t = 30,000$; all others are plotted to $T_c - 1$. The results can be summarized as follows.

The two largest lattices, $N \in \{536, 693\}$ were still decaying when the evolution was stopped at $t = 30,000$; since both of these lattices have $f_P = 0$ for the unperturbed case, we expect the noisy decay to have zero asymptotic value as well. On all other lattices, $f_P(t)$ decayed to zero at finite t. There was no leveling off to a nonzero asymptotic value; the decay profiles for all lattices followed the appropriate RMW curve all the way to $f_P = 0$. This difference is most significant in the case of the decelerating-decay (class IA) lattices $N \in \{42, 66, 94, 190\}$, two of which are in the worst-case set N_{wc}. These lattices actually took on the catastrophic profile of class IB. The RMW decay profile $f_{RMW}(t)$ for the worst-case lattice $N = 190$, plotted in fig. 13.5 as the dashed line curving down off the edge of the figure, shows a roughly constant offset from the noisy decay profile $f_P(t)$; there is no trace of the decelerating-decay behavior of the noise-free evolution. Neither the catastrophic-decay (class IB) lattices $N \in \{36, 536\}$ nor the odd-N (class II) lattices $N \in \{31, 45, 213, 693\}$ were significantly affected, up to the time when the unperturbed decay began to level off.

We interpret these results to indicate that the periodic orbits nearby, but not in, the attractors Λ^0 and $\Lambda^{0,0}$ are unstable to small perturbations. The detailed orbit structure imposed by the number-theoretic properties of the lattice size N is washed out by weak noise. Thus, the asymptotically nonattracted orbits in the Hamming vicinity are unstable: small perturbations typically drive the state into the attractor's basin. This is further evidence that Λ^0 and $\Lambda^{0,0}$ are attractors of ECA 18.

13.5 Subbasin Decay

To complete our investigation of the temporal stability properties of the attractors Λ^0 and $\Lambda^{0,0}$, we return to the subbasin vicinities $V_b(\Lambda^0)$ and $V_b(\Lambda^{0,0})$. Recall from section 12.1 that $V_b(\Lambda^0)$ consists of states with 0 or 2 dislocations, or equivalently, is the union of subbasins b_0 and b_2. Similarly, $V_b(\Lambda^{0,0})$ is the union of subbasins b_1 and b_3, respectively consisting of states having 1 and 3 dislocations, along with the pattern 0^* included for technical reasons. The subbasin vicinity corresponds to the smallest "excitation" of the system in the sense that the states have the minimal number of dislocations to move them off the attractor. In a parallel series of investigations on the same set of lattices as above, we calculated $f_P(t)$ for an initial ensemble of states drawn uniformly from subbasins b_2 or b_3, as appropriate. This induces a distribution of initial interdislocation distances that is uniform, rather than exponentially decaying, as was the case for V_H.

On all of the lattices measured, the convergence time T_c was the same for V_b as for V_H. On lattices where V_H had a vanishing asymptotic fraction f_P, V_b also had $f_P = 0$. On the remaining lattices, f_P was typically higher for V_b than for V_H. Unlike the Hamming vicinity profiles, the even-size lattices did not follow a common backbone. Instead, they formed a family of similarly-shaped curves parametrized by